HHS Public Access

Author manuscript

Angew Chem Int Ed Engl. Author manuscript; available in PMC 2015 December 15.

Published in final edited form as:

Angew Chem Int Ed Engl. 2014 December 15; 53(51): 14096–14101. doi:10.1002/anie.201408533.

Fluorine-18 labeled maltohexaose images bacterial infections by PET

Xinghai Ning[#],
Department of Bioengineering, UC Berkeley, 284 Hearst Memorial Mining Building, UC Berkeley, Berkeley, CA 94720 (USA)

Wonewoo Seo[#],
Department of Radiology and Imaging Sciences, Emory University (USA)

Seungjun Lee,
Department of Bioengineering, UC Berkeley, 284 Hearst Memorial Mining Building, UC Berkeley, Berkeley, CA 94720 (USA)

Kiyoko Takemiya,
Division of Cardiology, Department of Medicine, Emory University School of Medicine (USA)

Mohammad Rafi,
Department of Bioengineering, UC Berkeley, 284 Hearst Memorial Mining Building, UC Berkeley, Berkeley, CA 94720 (USA)

Xuli Feng,
Department of Bioengineering, UC Berkeley, 284 Hearst Memorial Mining Building, UC Berkeley, Berkeley, CA 94720 (USA)

Daiana Weiss,
Division of Cardiology, Department of Medicine, Emory University School of Medicine (USA)

Xiaojian Wang,
Department of Bioengineering, UC Berkeley, 284 Hearst Memorial Mining Building, UC Berkeley, Berkeley, CA 94720 (USA)

Larry Williams,
Department of Radiology and Imaging Sciences, Emory University (USA)

Vernon M. Camp,
Department of Radiology and Imaging Sciences, Emory University (USA)

Malveaux Eugene,
Department of Radiology and Imaging Sciences, Emory University (USA)

W. Robert Taylor,

Correspondence to: W. Robert Taylor.

[*] Fax: (+1) 510-642-5835 nmurthy@berkeley.edu, mgoodma@emory.edu.

Supporting information for this article is available on the WWW under http://dx.doi.org/10.1002/anie.201xxxxxx.

Division of Cardiology, Department of Medicine and the Department of Biomedical Engineering, Emory University School of Medicine and the Atlanta VA Medical Center (USA)

Mark Goodman[*], and
Department of Radiology and Imaging Sciences, Emory University (USA)

Niren Murthy[*]
Department of Bioengineering, UC Berkeley, 284 Hearst Memorial Mining Building, UC Berkeley, Berkeley, CA 94720 (USA)

[#] These authors contributed equally to this work.

Abstract

A new positron emission tomography (PET) tracer, composed of ^{18}F labeled maltohexaose (MH^{18}F), can image bacteria in vivo with a sensitivity and specificity that is orders of magnitude better than fluorodeoxyglucose (^{18}FDG). MH^{18}F can detect early stage infections composed of as few as 10^5 E.coli colony forming units (CFUs), and can identify drug resistance in bacteria in vivo. MH^{18}F has the potential to improve the diagnosis of bacterial infections given its unique combination of high specificity and sensitivity for bacteria.

Keywords

maltodextrin transporters; maltohexaose; radiochemistry; bacterial infections; positron emission tomography

The diagnosis of bacterial infections remains a central challenge in medicine. Infections are currently diagnosed via culturing of tissue biopsies or blood samples.[1] However these methods can only detect late stage infections that are challenging to treat. Bacterial infections therefore cause an enormous medical burden, for example, the mortality caused by bacterial infections was greater than the mortality caused from AIDs, breast cancer and prostate cancer combined.[2] Bacterial infections can be treated effectively, if diagnosed and treated at an early stage, and if the presence of drug resistance is also identified. However, this is challenging at present because the symptoms of infections look identical to a variety of other illnesses, such as cancer and inflammation.[3] Thus in this clinical environment, an imaging technology that can identify and localize bacterial infections with high sensitivity and specificity has the potential to have a significant impact on medicine.

Positron emission tomography (PET) imaging has the potential to significantly improve the diagnosis of bacterial infections due to its unparalleled sensitivity.[4] However, ^{18}FDG is currently the only PET contrast agent available for clinical imaging of infections, and is problematic because it lacks specificity for bacteria and has high uptake in mammalian cells.[5] ^{18}FDG therefore cannot distinguish bacterial infections from other pathologies such as cancer and inflammation, and cannot diagnose bacterial infections at an early stage.[5a, 6] Although numerous experimental PET contrast agents have been developed for imaging bacterial infections, such as radiolabeled antibiotics,[7] antimicrobial peptides,[1a] antibodies[8] or white blood cells,[9] these agents have had minimal clinical impact. Several factors have contributed to the lack of success of bacterial imaging agents, such as poor

clearance due to non-specific adsorption, low target receptor expression on bacteria, or complicated radiochemical synthesis, which are challenging to perform in clinical radiochemistry labs.[10] Therefore, there is a great need for the development of new PET contrast agents that can image small numbers of bacteria with high specificity *in vivo*.[11]

Herein, we present a new PET tracer, composed of ^{18}F labeled maltohexaose (MH^{18}F) that can image bacterial infections *in vivo* with unprecedented sensitivity and specificity (see Scheme 1). MH^{18}F targets the bacteria-specific maltodextrin transporter, which internalizes alpha 1,4 linked glucose oligomers (maltodextrins) as a source of glucose.[12] The maltodextrin transport system is an ideal target for imaging bacteria because of its high uptake of maltodextrins (K_m of 130 μM),[13] great specificity for bacteria, and the rapid clearance of maltodextrins from un-infected tissues.[14] In addition, the maltodextrin transporter is only functional in metabolically active bacteria and MH^{18}F uptake is therefore an indicator of bacterial viability,[14b, 15] and potentially antibiotic efficacy. Finally, MH^{18}F should have minimal toxicity in humans because maltodextrins are a commonly used food additive.[16]

A synthetic strategy was devised to synthesize MH^{18}F via nucleophilic 18-Fluorination of the maltohexaose-brosylate precursor (**3**) with K^{18}F in the presence of kryptofix k222 (see Scheme 1). The reducing end of maltohexaose was selected for fluorination because the maltodextrin transporter recognizes the non-reducing end of maltodextrins and should therefore tolerate substitutions at the reducing end.[17] Azide functionalized maltohexaose **1** was synthesized from maltohexaose in 4 steps following established methods,[14b] and was conjugated with pent-4-yn-1-yl 4-bromobenzenesulfonate **2** using the Cu(I) catalyzed Huisgen cycloaddition, to afford the brosylate-maltohexaose precursor **3**.[18] Radiochemical synthesis of MH^{18}F was carried with cryptate-mediated nucleophilic substitution of the brosylate precursor **3** with potassium ^{18}F-fluoride (K^{18}F), followed by basic hydrolysis with NaOH and acid neutralization. A decay corrected yield of 4.2% was obtained for this synthetic procedure, starting from ^{18}F-fluoride, with an 87 % radiochemical purity, based on radiometric HPLC (see Supplementary Figure S5).[19] The protocol for the synthesis of MH^{18}F had a synthesis time of 100 minutes, and follows the same procedures used to make ^{18}FDG,[20] and should therefore be achievable in clinical radiochemistry laboratories. In addition, we anticipate that the radiochemical yield of MH^{18}F can be increased using new F-18 fluorination methodologies.[19]

MH^{18}F is designed to selectively target bacteria due to the presence of maltodextrin transporters in bacteria, and their absence in mammalian cells. We therefore investigated if MH^{19}F has specificity for bacteria over mammalian cells, and if it is internalized via the maltodextrin transporter LamB, using F19-NMR. Bacteria (*E.coli)* and mammalian cells (hepatocytes) were incubated with a 500 μM concentration of MH^{19}F for one hour, washed with PBS, lysed, and the cellular supernatant was analyzed using F19-NMR. Figures 1a and 1b demonstrate that MH^{19}F has high specificity for bacteria over mammalian cells and is robustly internalized. For example, under these conditions, *E.coli* had accumulated 2 orders of magnitude more MH^{19}F than hepatocytes, and reached millimolar intracellular concentrations. In addition we performed maltohexaose competition experiments and experiments with LamB mutant *E.coli* to determine if MH^{19}F was being internalized via the

maltodextrin transport pathway. Figure 1a demonstrates that the uptake of $MH^{19}F$ in *E.coli* could be inhibited by an excess of maltohexaose, and that there is minimal uptake of $MH^{19}F$ in LamB mutants, demonstrating that $MH^{19}F$ enters *E.coli* via the maltodextrin transport pathway.

We investigated the ability of $MH^{18}F$ to image bacterial infections in rats. *E.coli* (10^7 CFUs) were injected into the left triceps muscle of rats, and the right triceps muscle was injected with PBS as a control. Two hours later, the rats were injected with 250 μCi of $MH^{18}F$ via the tail vein, and dynamic PET scans were performed using an Inveon micro PET/CT Preclinical Scanner (Siemens). Figures 2a and b demonstrates that $MH^{18}F$ clears well from healthy tissue but is retained in infected muscle. For example, bacterial infections were clearly visible as early as 10 min after $MH^{18}F$ injection and after seventy minutes had a high target-to-control contrast of 8.5, allowing bacterial infections to be easily visualized *in vivo*.

A key challenge in imaging bacteria is developing probes that have high sensitivity for bacteria.[21] Current PET tracers for imaging bacteria, such as ^{18}FDG and radiolabeled antibiotics and antibodies, can only image 10^7-10^9 bacterial CFUs *in vivo*, and cannot detect infections at an early stage.[22] $MH^{18}F$ has the potential to detect small numbers of bacteria because of its fast transport into bacteria and its rapid clearance from un-infected tissues. We investigated the ability of $MH^{18}F$ to image early stage bacterial infections. *E.coli* (10^5 CFUs) were injected into the left triceps muscle of rats and imaged with $MH^{18}F$ as described above. Figure 3b demonstrates that $MH^{18}F$ is capable of detecting as few as 10^5 bacterial CFUs *in vivo*, for example, rat triceps muscles infected with 10^5 bacterial CFUs had a 2.7 fold increase in radioactivity over un-infected controls. Thus, $MH^{18}F$'s unique combination of robust transport into bacteria and clearance from healthy tissues, allows it to image bacteria with high sensitivity.

^{18}FDG is currently the only PET radiopharmaceutical available for imaging bacterial infections; however, ^{18}FDG has significant limitations due to its high uptake in mammalian cells.[23] To determine the translational potential of $MH^{18}F$, a biodistribution study was performed with $MH^{18}F$ and ^{18}FDG to compare their specificity for bacteria and non-specific adsorption in healthy tissues. Rats were infected with 10^9 colony forming units (CFUs) of *E.coli* and intravenously injected with either $MH^{18}F$ or ^{18}FDG. After one hour post administration, the various organs were harvested and their radioactivty was measured. Figure 4 demonstrates that $MH^{18}F$ is specific for bacteria and has excellent clearance from healthy tissues. For example, $MH^{18}F$ generated a 30 fold difference in accumulation between infected muscles versus healthy muscles, and in contrast, ^{18}FDG generated only a 1.5 fold difference. The improved biodistribution pattern of $MH^{18}F$ over ^{18}FDG is due to the exclusive expression of maltohexaose transporters in bacteria in contrast to the high expression of glucose transporters in mammalian cells.[12c, 24] This allowed $MH^{18}F$ to clear from all of the major organs including heart, lung, brain, liver, bone and muscle, whereas ^{18}FDG had significant accumulation within these tissues. For example, in infected rats, the ratio of accumulation of $MH^{18}F$ in infected muscle versus liver was 5, whereas for ^{18}FDG, this ratio was only 0.3, and for other reported PET contrast agents the infected muscle to liver ratio is also generally less than 1.[1a, 7-8] The excellent clearance of $MH^{18}F$

allowed it to target bacteria much better than ^{18}FDG, and MH^{18}F therefore has the potential to image bacterial infections in a variety of anatomical areas.

At present, there is no direct method available to monitor the efficacy of antibiotic treatment, and doctors therefore have to rely on non-specific and imprecise clinical indicators to guide antibiotic therapy.[25] MH^{18}F has the potential to image bacterial drug resistance because it targets ATP binding cassette (ABC) transporters,[26] which require ATP for internalizing their substrates, connecting MH^{18}F's uptake with cellular metabolism and bacterial viability. We therefore investigated if MH^{18}F could distinguish between live versus dead bacteria and identify resistance to therapy. We first performed PET imaging with MH^{18}F and ^{18}FDG, and compared their ability to monitor bacterial metabolic activity *in vivo*. Rats were injected with 10^9 CFUs of live *E.coli* in their left triceps and 10^9 CFUs of metabolically inactive *E.coli* (sodium azide treated) in their right triceps. Two hours later, the rats were injected with 250 μCi of either MH^{18}F or ^{18}FDG via the tail vein, and imaged using an Inveon micro PET/CT Scanner. Figure 5a shows that MH^{18}F can distinguish between live versus metabolically inactive bacteria, for example metabolically active *E.coli* had a 7 fold increase in relative radioactivity over sodium azide treated metabolically inactive bacteria, demonstrating that MH^{18}F is being actively transported by bacteria *in vivo*. In contrast, Figure 5b shows that ^{18}FDG could not distinguish between live versus dead bacteria, due to its high uptake by inflammatory cells.

Based on these results we investigated if MH^{18}F could identify bacterial drug resistance *in vivo* and measure antibiotic efficacy. Rats were infected with ampicillin-resistant *E.coli* (10^9 CFUs) and wild-type *E.coli* (10^9 CFUs), treated with ampicillin and imaged with MH^{18}F. Figure 6a demonstrates that MH^{18}F can measure the efficacy of antibiotics *in vivo* and rapidly identify drug resistance. For example, ampicillin-resistant *E.coli* generated an 8.2 fold increase in PET signal intensity over susceptible *E.coli*, due to their increased survival under antibiotic treatment. In addition, we investigated if MH^{18}F could monitor the treatment of ampicillin resistant bacteria with ciprofloxacin, and be used as a real time methodology to assess antibiotic efficacy. Figure 6b demonstrates that in rats treated with ciprofloxacin, both ampicillin-resistant *E.coli* (10^9 CFUs) and wild-type *E.coli* (10^9 CFUs) infected tissues have very low accumulation of MH^{18}F, indicating that MH^{18}F can quantify the effects of antibiotics, and can be used to guide the selection of antibiotics.

In conclusion, in this report we present a bacterial targeted PET tracer, termed MH^{18}F, which can image bacteria *in vivo* with sensitivity and specificity that is orders of magnitude better than previously reported PET tracers. MH^{18}F can also identify drug resistance and can therefore potentially assist physicians in prescribing antibiotics. Finally, MH^{18}F can be synthesized in one radiochemical step from clinically available K^{18}F, and therefore has the potential to rapidly enter into clinical trials.

Supplementary Material

Refer to Web version on PubMed Central for supplementary material.

Acknowledgments

This project has been funded in part with Federal funds from the National Heart, Lung, and Blood Institute, National Institutes of Health, Department of Health and Human Services, under Contract No. NIH R01 1R01HL096796-02 (N.M.), NIH U01 268201000043C-0-0-1, NIH R211R21AI098799-01 (N.M.), NIH 7UM1AI068636-07 and NIH R01 AI088023-03.

References

1. a Lupetti A, Welling MM, Pauwels EK, Nibbering PH. Lancet Infect. Dis. 2003; 3:223–229. [PubMed: 12679265] b van Doorn LJ, Henskens Y, Nouhan N, Verschuuren A, Vreede R, Herbink P, Ponjee G, van Krimpen K, Blankenburg R, Scherpenisse J, Quint W. J. Clin. Microbiol. 2000; 38:13–17. [PubMed: 10618055]
2. a Lipsky BA, Itani K, Norden C. G. Linezolid Diabetic Foot Infections Study. Clin. Infect. Dis. 2004; 38:17–24. [PubMed: 14679443] b Mandell LA, Wunderink RG, Anzueto A, Bartlett JG, Campbell GD, Dean NC, Dowell SF, File TM Jr. Musher DM, Niederman MS, Torres A, Whitney CG. A. Infectious Diseases Society of, S. American Thoracic. Clin. Infect. Dis. 2007; 44(Suppl 2):S27–72. [PubMed: 17278083]
3. a Gillissen A, Paparoupa M. Clin. Respir. J. 2014b Sfanos KS, Isaacs WB, De Marzo AM. Am. J. Clin. Exp. Urol. 2013; 1:3–11. [PubMed: 25110720]
4. a Phelps ME. Proc. Natl. Acad. Sci. U. S. A. 2000; 97:9226–9233. [PubMed: 10922074] b Ametamey SM, Honer M, Schubiger PA. Chem. Rev. 2008; 108:1501–1516. [PubMed: 18426240]
5. a Glaudemans AW, Signore A. Eur. J. Nucl. Med. Mol. Imag. 2010; 37:1986–1991.b Erba PA, Bandera F, Sollini M, Tascini C. J. Am. Coll. Cardiol. 2012; 60:1435–1436. author reply 1437. [PubMed: 23036633] c Keidar Z, Nitecki S. Semin. Nucl. Med. 2013; 43:396–402. [PubMed: 23905620] d del Rosal T, Goycochea WA, Mendez-Echevarria A, Garcia-Fernandez de Villalta M, Baquero-Artigao F, Coronado M, Marin MD, Albajara L. Eur. J. Pediatr. 2013; 172:1111–1115. [PubMed: 23479196]
6. a Corstens FHM, van der Meer JWM. The Lancet. 1999; 354:765–770.b Gemmel F, Dumarey N, Welling M. Semin. Nucl. Med. 2009; 39:11–26. [PubMed: 19038597] c van Oosten M, Schäfer T, Gazendam JAC, Ohlsen K, Tsompanidou E, de Goffau MC, Harmsen HJM, Crane LMA, Lim E, Francis KP, Cheung L, Olive M, Ntziachristos V, van Dijl JM, van Dam GM. Nat. Commun. 2013:4.
7. Langer O, Muller U, Brunner M, Zeitlinger M, Joukhadar C, Mitterhauser M, Wadsak W, Kletter K, Muller M. Eur. J. Nucl. Med. Mol. Imag. 2004; 31:S447–S447.
8. a Rusckowski M, Gupta S, Liu G, Dou S, Hnatowich DJ. J. Nucl. Med. 2004; 45:1201–1208. [PubMed: 15235067] b Rennen HJ, Makarewicz J, Oyen WJ, Laverman P, Corstens FH, Boerman OC. Nucl. Med. Biol. 2001; 28:401–408. [PubMed: 11395313]
9. a Bhattacharya A, Kochhar R, Sharma S, Ray P, Kalra N, Khandelwal N, Mittal BR. J. Nucl. Med. 2014; 55:1267–1272. [PubMed: 24994930] b Jones HA, Peters AM, Clark JC. Nucl. Med. Commun. 2001; 22:601–602. [PubMed: 11388584]
10. a Petrik M, Haas H, Schrettl M, Helbok A, Blatzer M, Decristoforo C. Nucl. Med. Biol. 2012; 39:361–369. [PubMed: 22172389] b Langer O, Brunner M, Zeitlinger M, Ziegler S, Müller U, Dobrozemsky G, Lackner E, Joukhadar C, Mitterhauser M, Wadsak W, Minar E, Dudczak R, Kletter K, Müller M. Eur. J. Nucl. Med. Mol. Imag. 2005; 32:143–150.c Petruzzi N, Shanthly N, Thakur M. Semin. Nucl. Med. 2009; 39:115–123. [PubMed: 19187804] d Lu C, Jiang Q, Tan C, Tang J, Zhang J. Molecules. 2012; 17:8518–8532. [PubMed: 22801365]
11. Signore A, Mather SJ, Piaggio G, Malviya G, Dierckx RA. Chem. Rev. 2010; 110:3112–3145. [PubMed: 20415479]
12. a Shuman HA. Ann. Microbiol. (Paris). 1982; 133A:153–159. [PubMed: 7041738] b Klebba PE. Res. Microbiol. 2002; 153:417–424. [PubMed: 12405347] c Charbit A. Front. Biosci. 2003; 8:s265–274. [PubMed: 12700071] d Gopal S, Berg D, Hagen N, Schriefer EM, Stoll R, Goebel W, Kreft J. PLoS One. 2010; 5:e10349. [PubMed: 20436965] e Boos W, Shuman H. Microbiol. Mol. Biol. Rev. 1998; 62:204–229. [PubMed: 9529892]

13. a Dippel R, Boos W. J Bacteriol. 2005; 187:8322–8331. [PubMed: 16321936] b Freundlieb S, Ehmann U, Boos W. J Biol Chem. 1988; 263:314–320. [PubMed: 3275641]
14. a Reuss R, Ludwig J, Shirakashi R, Ehrhart F, Zimmermann H, Schneider S, Weber MM, Zimmermann U, Schneider H, Sukhorukov VL. J. Membr. Biol. 2004; 200:67–81. [PubMed: 15520905] b Ning X, Lee S, Wang Z, Kim D, Stubblefield B, Gilbert E, Murthy N. Nat. Mater. 2011; 10:602–607. [PubMed: 21765397]
15. Sharff AJ, Rodseth LE, Spurlino JC, Quiocho FA. Biochemistry. 1992; 31:10657–10663. [PubMed: 1420181]
16. Shepherd R, Robertson A, Ofman D. Food Hydrocolloid. 2000; 14:281–286.
17. a Dippel R, Boos W. J. Bacteriol. 2005; 187:8322–8331. [PubMed: 16321936] b Freundlieb S, Ehmann U, Boos W. J. Biol. Chem. 1988; 263:314–320. [PubMed: 3275641]
18. a Wang Q, Chan TR, Hilgraf R, Fokin VV, Sharpless KB, Finn MG. J. Am. Chem. Soc. 2003; 125:3192–3193. [PubMed: 12630856] b Kolb HC, Finn MG, Sharpless KB. Angew. Chem. 2001; 113:2056–2075.Angew. Chem. Int. Ed. 2001; 40:2004–2021.
19. a O'Hagan D, Schaffrath C, Cobb SL, Hamilton JT, Murphy CD. Nature. 2002; 416:279. [PubMed: 11907567] b Kim DW, Choe YS, Chi DY. Nucl. Med. Biol. 2003; 30:345–350. [PubMed: 12767390] c Kim DW, Chi DY. Angew. Chem. 2004; 116:489–491.Angew. Chem. Int. Ed. 2004; 43:483–485.d Kim DW, Ahn DS, Oh YH, Lee S, Kil HS, Oh SJ, Lee SJ, Kim JS, Ryu JS, Moon DH, Chi DY. J. Am. Chem. Soc. 2006; 128:16394–16397. [PubMed: 17165796] e Glaser M, Arstad E. Bioconjugate Chem. 2007; 18:989–993.f Vaidyanathan G, Zalutsky MR. Nucl. Med. Biol. 1992; 19:275–281.g Iwata R, Pascali C, Bogni A, Horvath G, Kovacs Z, Yanai K, Ido T. Appl. Radiat. Isot. 2000; 52:87–92. [PubMed: 10670927] h Prante O, Einsiedel J, Haubner R, Gmeiner P, Wester HJ, Kuwert T, Maschauer S. Bioconjugate Chem. 2007; 18:254–262.i Ting R, Adam MJ, Ruth TJ, Perrin DM. J. Am. Chem. Soc. 2005; 127:13094–13095. [PubMed: 16173707] j Lee E, Kamlet AS, Powers DC, Neumann CN, Boursalian GB, Furuya T, Choi DC, Hooker JM, Ritter T. Science. 2011; 334:639–642. [PubMed: 22053044] k Lee E, Hooker JM, Ritter T. J. Am. Chem. Soc. 2012; 134:17456–17458. [PubMed: 23061667] l Huiban M, Tredwell M, Mizuta S, Wan Z, Zhang X, Collier TL, Gouverneur V, Passchier J. Nat. Chem. 2013; 5:941–944. [PubMed: 24153372]
20. a Surasi DS, Bhambhvani P, Baldwin JA, Almodovar SE, O'Malley JP. J. Nucl. Med. Technol. 2014; 42:5–13. [PubMed: 24503347] b Nakao R, Ito T, Yamaguchi M, Suzuki K. Nucl. Med. Biol. 2008; 35:239–244. [PubMed: 18312835]
21. a Bettegowda C, Foss CA, Cheong I, Wang Y, Diaz L, Agrawal N, Fox J, Dick J, Dang LH, Zhou S, Kinzler KW, Vogelstein B, Pomper MG. Proc. Natl. Acad. Sci. U. S. A. 2005; 102:1145–1150. [PubMed: 15653773] b Smith BA, Akers WJ, Leevy WM, Lampkins AJ, Xiao S, Wolter W, Suckow MA, Achilefu S, Smith BD. J. Am. Chem. Soc. 2009; 132:67–69. [PubMed: 20014845]
22. a Pellegrino D, Bonab AA, Dragotakes SC, Pitman JT, Mariani G, Carter EA. J. Nucl. Med. 2005; 46:1522–1530. [PubMed: 16157536] b Fischman AJ, Livni E, Babich J, Alpert NM, Liu YY, Thom E, Cleeland R, Prosser BL, Callahan RJ, Correia JA. Antimicrob. Agents Chemother. 1992; 36:2286–2292. [PubMed: 1444310]
23. a Varagnolo L, Stokkel MPM, Mazzi U, Pauwels EKJ. Nucl. Med. Biol. 2000; 27:103–112. [PubMed: 10773538] b Hanasono MM, Kunda LD, Segall GM, Ku GH, Terris DJ. Laryngoscope. 1999; 109:880–885. [PubMed: 10369275] c Lind P, Igerc I, Beyer T, Reinprecht P, Hausegger K. Eur. J. Nucl. Med. Mol. Imag. 2004; 31:S125–S134.d Lubezky N, Metser U, Geva R, Nakache R, Shmueli E, Klausner JM, Even-Sapir E, Figer A, Ben-Haim M. J. Gastrointest. Surg. 2007; 11:472–478. [PubMed: 17436132]
24. a Strauss LG, Koczan D, Klippel S, Pan L, Willis S, Sachpekidis C, Dimitrakopoulou-Strauss A. Am. J. Nucl. Med. Mol. Imaging. 2013; 3:417–424. [PubMed: 24116350] b Deron P, Vangestel C, Goethals I, De Potter A, Peeters M, Vermeersch H, Van de Wiele C. Nuklearmedizin. 2011; 50:15–21. [PubMed: 21052609] c Wandersman C. Ann. Microbiol. (Paris). 1982; 133A:161–163. [PubMed: 7041739]
25. Roberts JA, Norris R, Paterson DL, Martin JH. Br. J. Clin. Pharmacol. 2012; 73:27–36. [PubMed: 21831196]
26. Morbach S, Tebbe S, Schneider E. J. Biol. Chem. 1993; 268:18617–18621. [PubMed: 8360157]

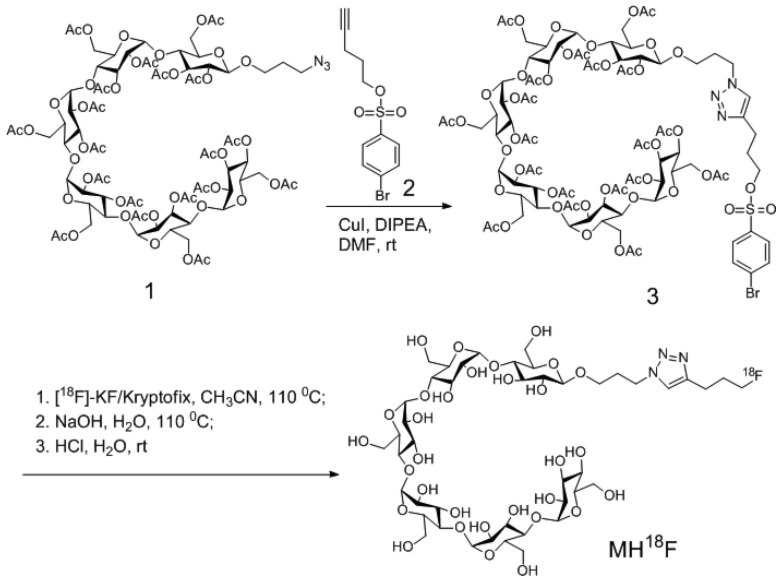

Scheme 1.

Synthesis of MH^{18}F. MH^{18}F is composed of ^{18}F-fluoride conjugated to maltohexaose and was synthesized by one-step nucleophilic ^{18}F-fluorination of brosylate-maltohexaose 3.

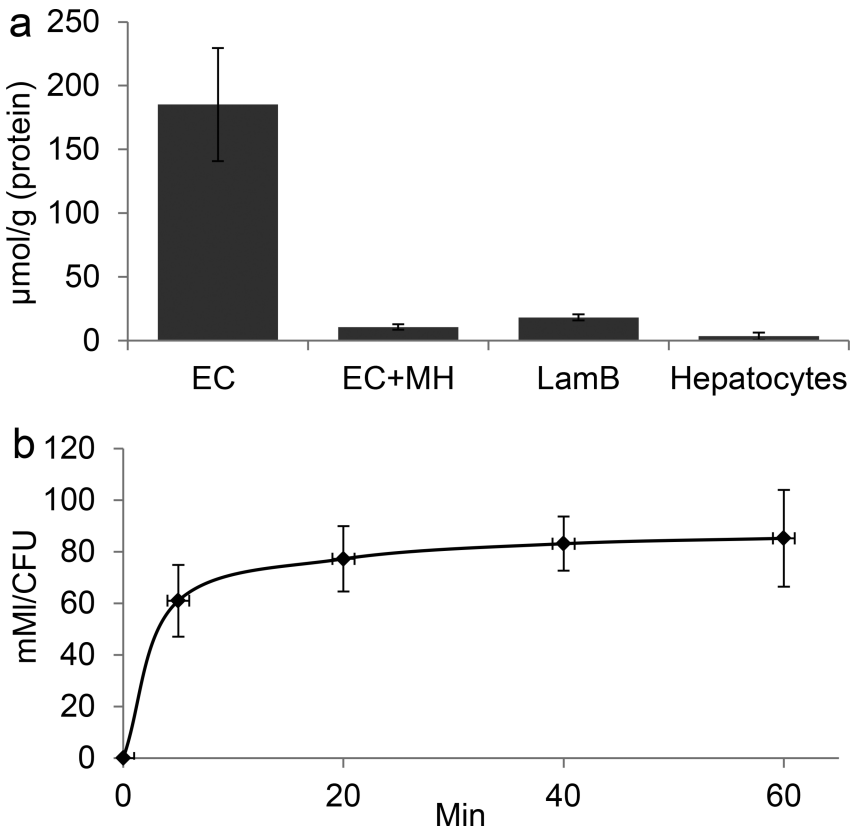

Figure 1.

$MH^{19}F$ has high specificity for bacteria and is robustly internalized by bacteria. **a**, $MH^{19}F$ has high specificity for bacteria over hepatocytes. *E. coli* (EC), EC with LamB mutation (LamB) and mammalian cells were incubated with 500 μM $MH^{19}F$ for 1 hour in the presence or absence of 50 mM maltohexaose (MH). The intracellular $MH^{19}F$ concentration was determined and normalized to protein content. Bacteria robustly accumulate $MH^{19}F$ whereas hepatocytes have negligible uptake. The uptake of $MH^{19}F$ in EC is inhibited by a large excess of maltohexaose, and the uptake of $MH^{19}F$ in LamB mutants is significantly reduced. The results are expressed as mean micromoles per gram of protein ± s.e.m. for n = 3 per group. **b**, The accumulation of $MH^{19}F$ in EC reaches millimolar concentrations. EC were incubated with 500 μM $MH^{19}F$, and the intracellular concentration of $MH^{19}F$ was determined at different time points, n = 3 per group.

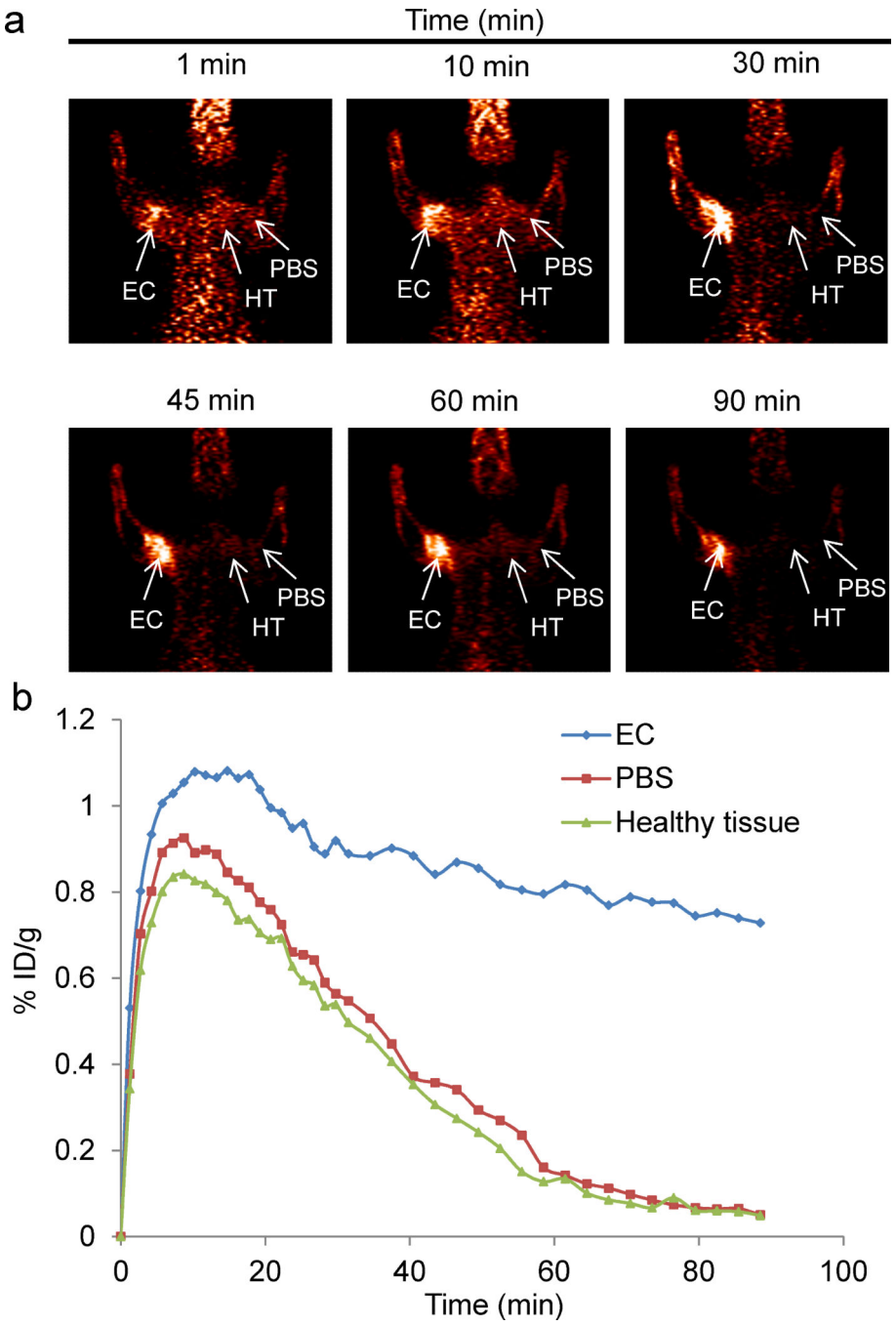

Figure 2.

In vivo PET imaging of rats infected with *E.coli* (10^7CFUs). **a.** Rats were infected in the left triceps muscle with 10^7 *E.coli*, injected with MH^{18}F, and dynamic PET scans were performed for 90 minutes using a microPET/CT. Infected muscles can be easily visualized after 90 min. **b.** Time activity curves of decay-corrected MH^{18}F activity in the infected rat, generated from Figure 2a. Infected muscle has an 8.5 fold increase in radioactivity over PBS injected muscle. Arrows indicate the location of infected muscle (EC), PBS injected muscle (PBS) and healthy tissue (HT).

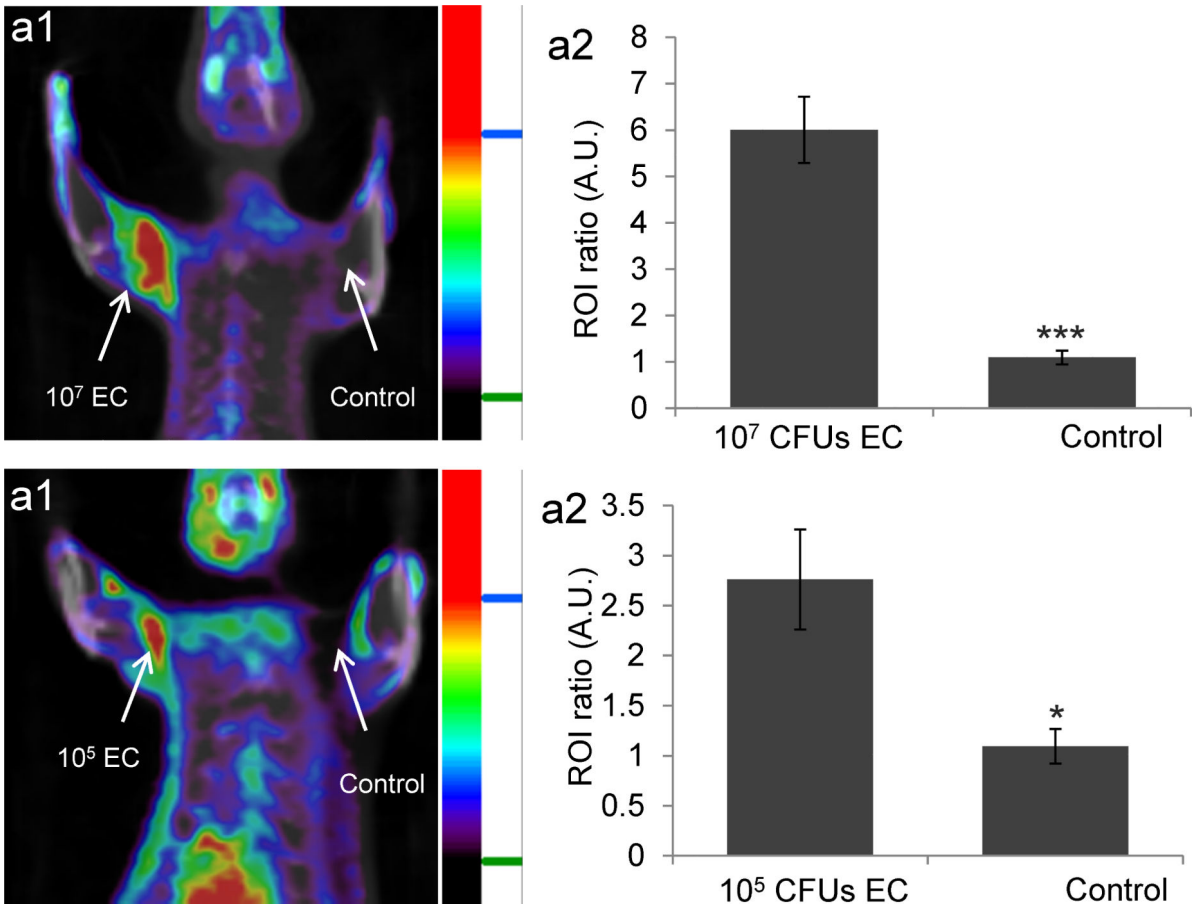

Figure 3.

$MH^{18}F$ can detect as few as 10^5 CFUs of *E.coli* (EC) in muscle infections. a1, $MH^{18}F$ can detect 10^7 *E.coli* CFUs in rats. Rats were infected with 10^7 *E.coli* and imaged with $MH^{18}F$ using a microPET/CT. The rat image is a representative result of four experiments, and identifies the infection site. a2, $MH^{18}F$ generates a 6 fold increase in radioactivity in infected muscles. b1, $MH^{18}F$ can detect as few as 10^5 *E.coli* in rats. Rats were infected with 10^5 *E.coli* CFUs and imaged with $MH^{18}F$ using a microPET/CT. The rat image is a representative result of four experiments, and identifies the infection site. b2, $MH^{18}F$ generates a 2.7 fold increase in radioactivity in infected muscles. Regions of interest (ROIs) including the infected muscles (target) or PBS injection areas (control) and healthy tissues (background) were identified and integrated using ASI Pro VM™ micro PET analysis software. The results in a2 and b2 are expressed as the target or control to background ratio (ROI ratio) ± s.e.m. for n = 4 per group. The ROI ratio is defined as the mean radioactivity in the target/the mean radioactivity in the background. The statistical significances in a2 and b2 were determined using a two-sample Student's *t*-test (*$p \leq 0.05$ and ***$p \leq 0.001$).

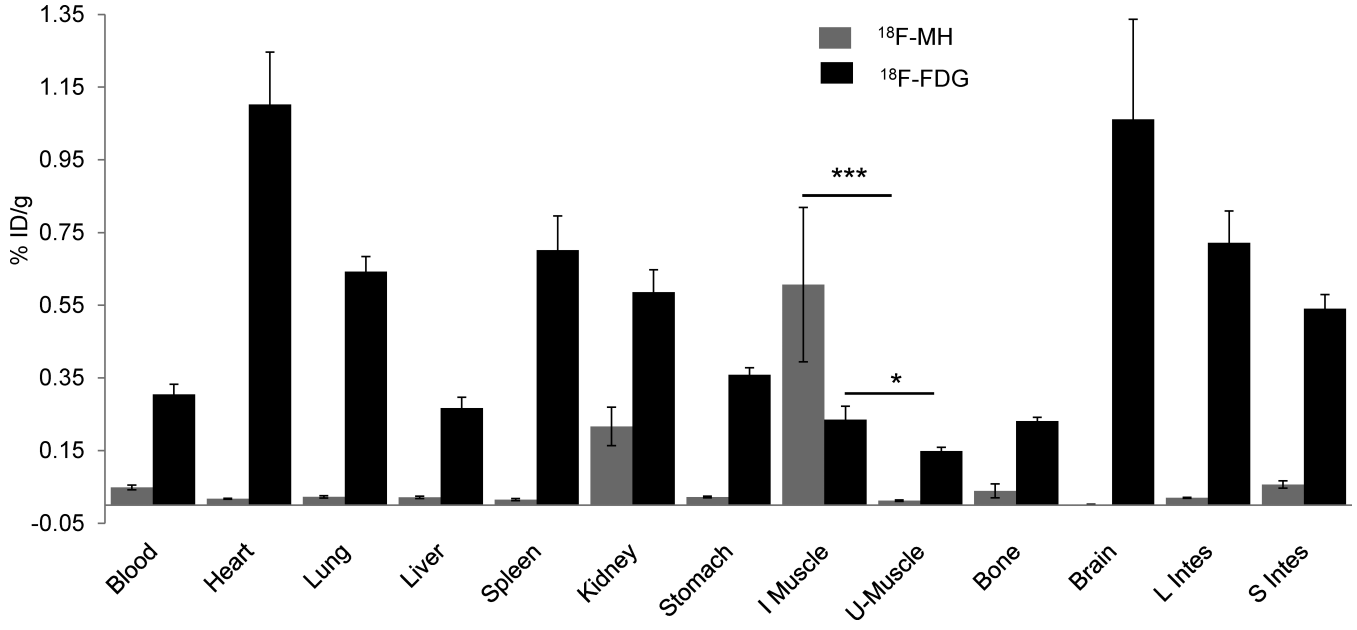

Figure 4.

$MH^{18}F$ is more effective than ^{18}FDG at imaging bacterial infections. A biodistribution study was performed with either $MH^{18}F$ or ^{18}FDG in rats infected with 10^9 *E.coli* CFUs. $MH^{18}F$ is efficiently cleared from un-infected tissues, whereas ^{18}FDG has significant accumulation within the major organs. The results are expressed as % injected dose/gram tissue ± s.e.m. for n = 4 per group. Statistical significance was determined using a two-sample Student's *t*-test (*$p \leq 0.05$ and ***$p \leq 0.001$).

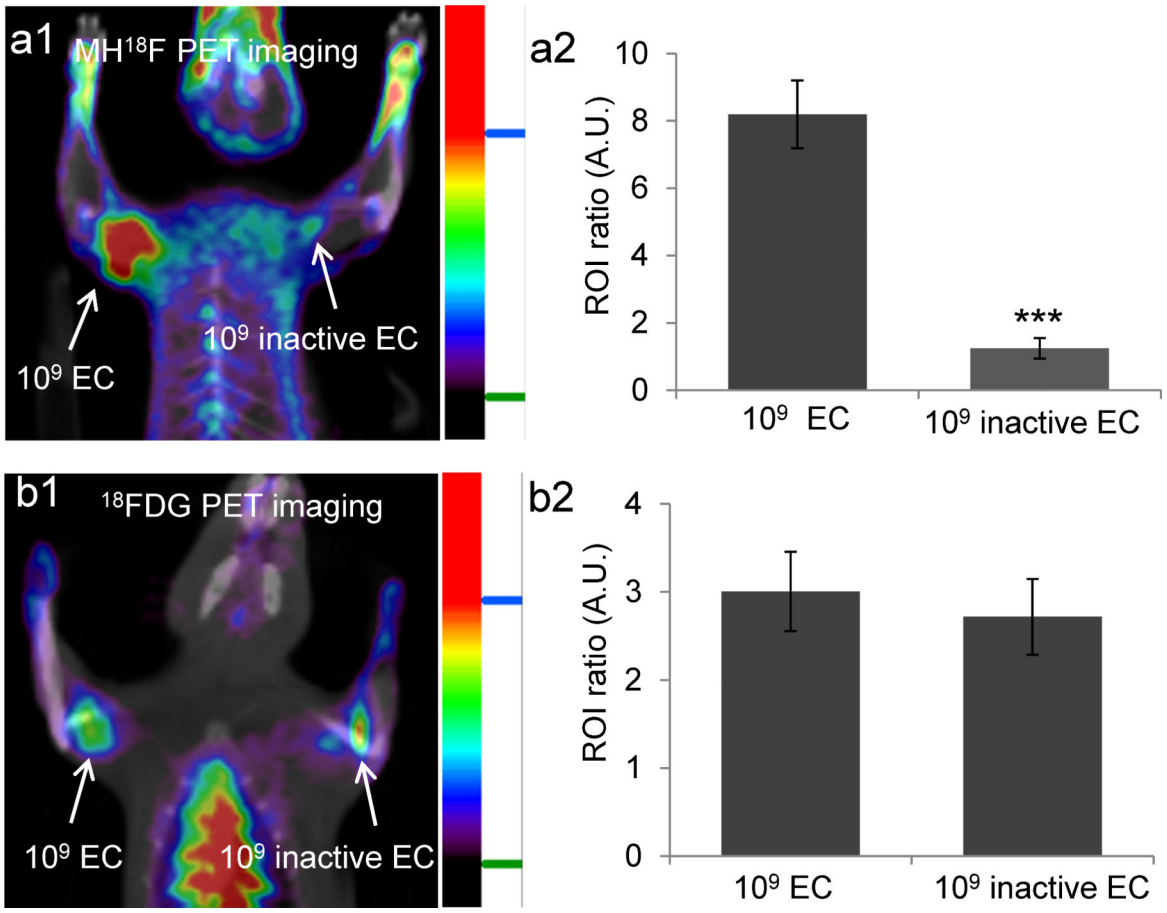

Figure 5.

MH^{18}F can distinguish between live versus dead bacteria and can discriminate infections from inflammation. **a1**, MH^{18}F can distinguish between live versus dead bacteria *in vivo*. Rats were infected with 10^9 live and dead *E.coli* and imaged with MH^{18}F using a microPET/CT. The rat image is a representative result of four experiments, and demonstrates that MH^{18}F does not accumulate in dead bacteria. **a2,** *E.coli* infected tissues had a 7 fold increase in radioactivity over muscles treated with dead bacteria. **b1**, ^{18}FDG cannot distinguish between live and dead *E.coli* infected tissues. Rats were infected with 10^9 live and dead *E.coli* CFUs and imaged with ^{18}FDG using a microPET/CT. The image is a representative result of four experiments, and demonstrates that ^{18}FDG cannot discriminate live bacteria from dead bacteria. **b2,** ^{18}FDG accumulates in both live and dead bacteria infected tissues. ROIs including the infected muscles (target) and healthy tissues (background) from **a1** and **b1**were identified and integrated using ASI Pro VM™ micro PET analysis software. The results in **a2** and **b2** are expressed as ROI ratio ± s.e.m. for n = 4 per group. The ROI ratio is defined as the mean radioactivity in the target/the mean radioactivity in the background. The statistical significance in **a2** was determined using a two-sample Student's *t*-test (***$p \leq 0.001$).

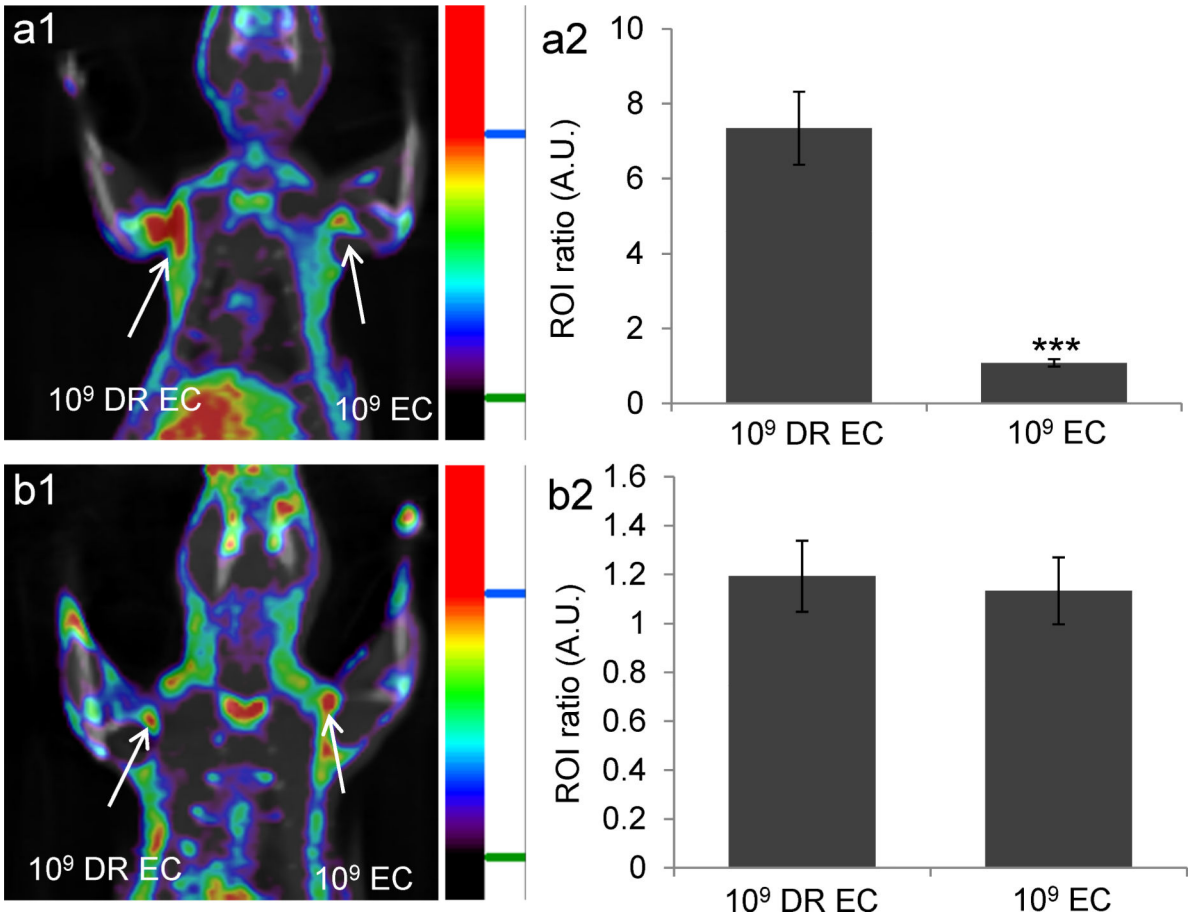

Figure 6.

$MH^{18}F$ can measure drug resistance and monitor the therapeutic effect of antibiotics *in vivo*. **a1**, $MH^{18}F$ can identify drug resistance in bacteria *in vivo*. Rats were infected with 10^9 CFUs of ampicillin-resistant *E.coli* (DR EC) and wild-type *E.coli* (EC), treated with ampicillin and imaged with $MH^{18}F$ using a microPET/CT. The rat image is a representative result of four experiments, and demonstrates that $MH^{18}F$ only accumulates in DR EC infected muscles. **a2**, DR EC generated a 10 fold increase in radioactivity over EC. **b1**, $MH^{18}F$ can monitor the therapeutic effect of antibiotics. Rats were infected with DR EC and EC, treated with ciprofloxacin and imaged with $MH^{18}F$ using a microPET/CT. The rat image is a representative result of four experiments, and demonstrates that both DR EC and EC infected muscles have weak accumulation of $MH^{18}F$. **a2**, Both infected tissues have weak radioactivity. ROIs including the infected muscles (target) and healthy tissues (background) from **a1** and **b1** were identified and integrated using ASI Pro VM™ micro PET analysis software. The results in **a2** and **b2** are expressed as ROI ratio ± s.e.m. for n = 4 per group. The ROI ratio is defined as the mean radioactivity in the target/the mean radioactivity in the background. The statistical significance in **a2** was determined using a two-sample Student's *t*-test (***$p \leq 0.001$).